



UNIVERSITY OF LEEDS

This is a repository copy of *Musculoskeletal Model-Based Adaptive Variable Impedance Control With Flexible Prescribed Performance for Rehabilitation Robots*.

White Rose Research Online URL for this paper:

<https://eprints.whiterose.ac.uk/226818/>

Version: Accepted Version

---

**Article:**

Cao, Y. [orcid.org/0000-0002-3486-5518](https://orcid.org/0000-0002-3486-5518), Ma, S. [orcid.org/0009-0008-4808-1221](https://orcid.org/0009-0008-4808-1221), Zhang, M. [orcid.org/0000-0002-0603-5525](https://orcid.org/0000-0002-0603-5525) et al. (4 more authors) (2025) Musculoskeletal Model-Based Adaptive Variable Impedance Control With Flexible Prescribed Performance for Rehabilitation Robots. IEEE/ASME Transactions on Mechatronics. ISSN 1083-4435

<https://doi.org/10.1109/tmech.2025.3562670>

---

This is an author produced version of an article accepted for publication in IEEE/ASME Transactions on Mechatronics made available under the terms of the Creative Commons Attribution License (CC-BY), which permits unrestricted use, distribution and reproduction in any medium, provided the original work is properly cited.

**Reuse**

This article is distributed under the terms of the Creative Commons Attribution (CC BY) licence. This licence allows you to distribute, remix, tweak, and build upon the work, even commercially, as long as you credit the authors for the original work. More information and the full terms of the licence here:

<https://creativecommons.org/licenses/>

**Takedown**

If you consider content in White Rose Research Online to be in breach of UK law, please notify us by emailing [eprints@whiterose.ac.uk](mailto:eprints@whiterose.ac.uk) including the URL of the record and the reason for the withdrawal request.



[eprints@whiterose.ac.uk](mailto:eprints@whiterose.ac.uk)  
<https://eprints.whiterose.ac.uk/>

# Musculoskeletal Model-Based Adaptive Variable Impedance Control with Flexible Prescribed Performance for Rehabilitation Robots

Yu Cao, *Member, IEEE*, Shuhao Ma, Mengshi Zhang, Zijian Li, Jindong Liu, Jian Huang, *Senior Member, IEEE* and Zhiqiang Zhang, *Senior Member, IEEE*

**Abstract**—In rehabilitation robotics, both compliance and high-precision motion are critical to effective rehabilitation training. However, there is an inherent conflict between system compliance and control accuracy, which presents significant challenges in achieving optimal performance. To address this issue, this paper proposes a surface electromyogram (sEMG)-driven musculoskeletal model-based adaptive variable impedance controller with flexible prescribed performance, ensuring a balance between compliance and precision motion in the human-robot interaction. We begin by formulating a constrained human-robot system and subsequently transform it into an unconstrained system using prescribed performance techniques. A novel impedance model is introduced to ensure system stability while maintaining prescribed performance. Furthermore, the controller integrates the Joint Strength Index (JSI), derived from an sEMG-driven musculoskeletal model, and incorporates a flexible prescribed performance function combined with adaptive stiffness and damping. The method supports both robot-dominant and human-dominant modes, and the seamless transition between them. Our findings show that lower human involvement increases system stiffness and narrows motion constraints, enabling high-precision motion. In contrast, greater human participation improves system compliance and broadens motion constraints, allowing for more freedom of movement. Finally, experiments were conducted on an upper-limb rehabilitation robot to validate the proposed method.

**Index Terms**—Rehabilitation robots, flexible prescribed performance, adaptive variable impedance, musculoskeletal model.

## I. INTRODUCTION

**S**TROKE has emerged as one of the most significant causes of disability worldwide [1], [2]. In recent years, the rehabilitation field has witnessed remarkable advances in robotic

therapy [3]–[5], which can offer personalized approaches based on the specific needs of patients and their recovery stages. In this context, active robot-assisted rehabilitation encourages patients to actively participate in rehabilitation exercises, facilitating motor relearning and the regaining of voluntary control [6]. The human active involvement implies that the robot should dynamically adjust its behavior based on the user’s intentions, providing assistance and complementing the user’s motions. One effective approach is impedance control, which incorporates compliance into the robot’s response, enabling it to adaptively regulate support levels across different movement phases, thereby enhancing both adaptability and interaction performance [7], [8]. However, traditional impedance control methods, which rely on fixed stiffness and damping, often struggle to adapt to changing patient conditions, leading to low control accuracy.

Prescribed Performance Control (PPC) may be a remedial approach, ensuring that the system consistently meets predefined error convergence criteria and performance metrics by introducing a prescribed performance function and an error transformation [9]–[11]. This approach enables high-precision control of the system by defining a narrowly constrained range. Therefore, integrating the advantages of impedance control and prescribed performance holds promise for significantly enhancing control performance. Irawan et al. [12] improved the performance of position-based impedance control on servo pneumatic system in rod-piston tracking. Gu et al. [13] developed a predefined-time impedance controller with prescribed performance for free-flying flexible-joint space robots to facilitate compliant target capture. Meng et al. [14] implemented a simple combination of prescribed performance and admittance control to enhance the dynamic response of the system. However, achieving high-precision motion often requires sufficient stiffness, creating an inherent conflict between system compliance and control accuracy. This challenge persists in effectively integrating impedance control with prescribed performance techniques.

Variable impedance could be an effective solution to the aforementioned issue. But system impedance varies with tasks, as seen in common rehabilitation applications. For instance, assist-as-needed (AAN) strategies exemplify impedance modulation by ensuring that the robotic system intervenes only when the subject cannot complete the movement independently [15], [16]. Under this principle, AAN dynamically ad-

Manuscript received Month xx, 2xxx; revised Month xx, xxxx; accepted Month x, xxxx. This work was supported in part by the U.K. Research and Innovation (UKRI) Horizon Europe Guarantee under Grant EP/Z001234/1 and Grant EP/Y027930/1, in part by the Royal Society under Grant IEC/NSF/211360, and in part by National Natural Science Foundation of China under Grant 62103157, 62333007, U24A20280, and 62233007. (Yu Cao and Shuhao Ma contributed equally to this work.) (Corresponding authors: Jian Huang, Jindong Liu and Zhiqiang Zhang)

Y. Cao, S. Ma and Z. Zhang are with the School of Electronic & Electrical Engineering, University of Leeds, Leeds, UK (e-mail: y.cao1@leeds.ac.uk, elsma@leeds.ac.uk, z.zhang3@leeds.ac.uk)

J. Huang and M. Zhang are with the Hubei Key Laboratory of Brain-inspired Intelligent Systems, School of Artificial Intelligence and Automation, Huazhong University of Science and Technology, Wuhan, China (e-mail: huang\_jan@mail.hust.edu.cn, dream\_poem@hust.edu.cn).

J. Liu and Z. Li are with ESTUN Medical Technology Ltd., Nanjing, China (e-mail: liujindong@estun.com, lizijian@estun.com).

justs the robot's stiffness and damping to divide the movement into two distinct components: a subject-driven part, where the patient actively controls the motion, and a robot-driven part, where the system provides assistance [17]. Duschau-Wicke et al. [18] presented a path control strategy with adjustable stiffness via virtual walls, enabling patients to influence the timing of their leg movements along a physiologically meaningful path. Agarwal et al. [19] and Asl et al. [20] respectively proposed force field and velocity field control strategies by integrating an offline-trained neural network model to determine the required torques. Garcia-Hernandez et al. [21] and Cao et al. [22] constructed weighted functions by using interaction force or sEMG signals to reflect subjects' participation, and proposed position-based control methods to achieve the assist-as-needed concept. However, the above methods either neglect position constraints or only consider fixed constraints, which still sacrifices the precision performance. This raises an additional challenge in designing the robot's impedance variations to effectively address the demands of ANN-based rehabilitation scenarios, while balancing prescribed performance requirements to achieve motion control that ensures both compliance and precise motion in the human-robot interactions.

Impedance learning is a promising approach [23], [24], with Learning from Demonstration (LfD) [25], [26] and reinforcement learning [27]–[29] being two common methods. However, these techniques often require large datasets and extensive training times, making them challenging to be deployed in real-world applications. Moreover, the training process is computationally expensive and time-consuming, further hindering their practical use. Alternatively, some approaches focus on directly constructing the learning rate for impedance, offering a potentially more efficient solution. Yang et al. [30] introduced a model-based spatial repetitive impedance learning method with variable iteration lengths in the time domain. Similarly, Sharifi et al. [31] developed adaptive laws for robot stiffness and damping to enable real-time impedance adjustment based on human behaviors. However, these methods primarily focus on ensuring system stability, and often overlook the complexities of the human-robot interaction, limiting the adaptability and responsiveness required for effective and intuitive human-robot interaction systems.

To address the aforementioned issues, this paper proposes a musculoskeletal model-based adaptive variable impedance controller with flexible prescribed performance for rehabilitation robots. The main contributions are as follows: 1) A novel impedance model that integrates prescribed performance with impedance control to maintain position transformation while ensuring system stability; 2) The design of a JSI-based flexible prescribed performance, along with adaptive variable stiffness and damping, using an sEMG-driven musculoskeletal model to balance tracking accuracy and compliance in the human-robot interaction; 3) Various experimental tests confirming the effectiveness of the proposed method.

## II. PROBLEM FORMULATION

For an  $n$ -DOF robotic manipulator interacting with a human at its end-effector, the dynamics in Cartesian space are:

$$M_x \ddot{\mathbf{x}} + C_x \dot{\mathbf{x}} + \mathbf{g}_x = \mathbf{F}_\tau + \mathbf{F}_{ext} \quad (1)$$

where  $\mathbf{x} = f(\mathbf{q}) \in \mathbb{R}^m$  is the coordinates of the configuration of the end-effector.  $\mathbf{q} \in \mathbb{R}^n$  is the joint configurations.  $\mathbf{F}_{ext} \in \mathbb{R}^m$  represent the human-robot interaction force applied to the robot.  $\mathbf{F}_\tau \in \mathbb{R}^m$  is the input vector related to the motor input torques  $\boldsymbol{\tau} = \mathbf{J}(\mathbf{q})^T \mathbf{F}_\tau$  with the Jacobian  $\mathbf{J}(\mathbf{q}) \in \mathbb{R}^{m \times n}$ .  $\mathbf{g}_x \in \mathbb{R}^m$  is the gravity vector.  $M_x \in \mathbb{R}^{m \times m}$  and  $C_x \in \mathbb{R}^{m \times m}$  are inertial matrix and centrifugal and Coriolis matrix.

**Property 1.** *The inertia matrix  $M_x$  is symmetric and positive definite:  $M_x = M_x^T > 0$ .*

**Property 2.** *The matrix  $\dot{M}_x - 2C_x$  is skew-symmetric and fulfills the condition:*

$$\mathbf{p}^T (\dot{M}_x - 2C_x) \mathbf{p} = 0, \forall \mathbf{p} \in \mathbb{R}^m \quad (2)$$

## III. IMPEDANCE CONTROL WITH PRESCRIBED PERFORMANCE

### A. Error Transformation

Let  $\mathbf{x}_d \in \mathbb{R}^m$  be the desired trajectory with the bounded  $\|\mathbf{x}_d\|$ ,  $\|\dot{\mathbf{x}}_d\|$  and  $\|\ddot{\mathbf{x}}_d\|$ . The tracking error  $\mathbf{e}_x = \mathbf{x} - \mathbf{x}_d$  is constrained if each element  $e_{xi}(t)$  of  $\mathbf{e}_x$  satisfies the following:

$$\underline{\xi}_i(t) < e_{xi}(t) < \bar{\xi}_i(t), \forall t \quad (3)$$

where  $\bar{\xi}_i(t)$  and  $\underline{\xi}_i(t)$  represent the upper and lower bounds, respectively, defined as  $\bar{\xi}_i(t) = -\underline{\xi}_i(t) = \mu_i \rho_i(t)$ , with  $\mu_i$  being a positive constant and  $\rho_i(t) = (\rho_{i0} - \rho_{i\infty}) \exp(-k_i t) + \rho_{i\infty}$  ( $\rho_{i0} > \rho_{i\infty}$ ). Given a transformation function  $-\mu_i < \varphi(z_i) = \mu_i \tanh(z_i) < \mu_i$ , the constrained problem can be converted into an unconstrained one with  $\lim_{z_i \rightarrow \infty} \varphi(z_i) = \mu_i$  and  $\lim_{z_i \rightarrow -\infty} \varphi(z_i) = -\mu_i$ . Let  $\xi_i = \bar{\xi}_i$ , the transformed error  $z_i$  with respect to  $e_{xi}$  is expressed as:

$$z_i = \text{In} \frac{\xi_i + e_{xi}}{\xi_i - e_{xi}}, \dot{z}_i = \frac{1}{\psi_i} \dot{e}_{xi} + \omega_i \quad (4)$$

where  $0 < \psi_i = \frac{\xi_i^2 - e_{xi}^2}{\xi_i} < \xi_i$ ,  $\omega_i = -\frac{e_{xi}}{\xi_i^2 - e_{xi}^2} \dot{\xi}_i$ . Hence, the relationship between  $\dot{\mathbf{e}}_x$  and  $\dot{\mathbf{z}}$  are denoted by:

$$\dot{\mathbf{e}}_x = \Psi \dot{\mathbf{z}} - \boldsymbol{\omega}_\psi, \ddot{\mathbf{e}}_x = \Psi \ddot{\mathbf{z}} + \dot{\Psi} \dot{\mathbf{z}} - \dot{\boldsymbol{\omega}}_\psi \quad (5)$$

where  $\Psi = \text{diag}\{\psi_1, \dots, \psi_m\} \in \mathbb{R}^{m \times m}$ ,  $\boldsymbol{\omega} = [\omega_1, \dots, \omega_m]^T \in \mathbb{R}^m$ ,  $\boldsymbol{\omega}_\psi = \Psi \boldsymbol{\omega} = [-\frac{\dot{\xi}_1}{\xi_1} e_{x1}, \dots, -\frac{\dot{\xi}_m}{\xi_m} e_{xm}]^T \in \mathbb{R}^m$ . Substituting (5) into (1), the dynamics of the robotic manipulator with prescribed performance is rewritten as:

$$M_z \ddot{\mathbf{z}} + C_z \dot{\mathbf{z}} + \mathbf{g}_z = \mathbf{F}_z + \mathbf{F}_{ez} + \mathbf{F}_\omega \quad (6)$$

where  $M_z = \Psi^T M_x \Psi \in \mathbb{R}^{m \times m}$ ,  $C_z = \Psi^T M_x \dot{\Psi} + \Psi^T C_x \Psi \in \mathbb{R}^{m \times m}$  and  $\mathbf{g}_z = \Psi^T \mathbf{g}_x \in \mathbb{R}^m$ ,  $\mathbf{F}_\omega = M_z \dot{\boldsymbol{\omega}} + C_z \boldsymbol{\omega} - \Psi^T (M_x \ddot{\mathbf{x}}_d + C_x \dot{\mathbf{x}}_d) \in \mathbb{R}^m$ .  $\mathbf{F}_z = \Psi^T \mathbf{F}_\tau \in \mathbb{R}^m$  and  $\mathbf{F}_{ez} = \Psi^T \mathbf{F}_{ext} \in \mathbb{R}^m$  are the transformed motor torque and human-robot interaction torque.

**Lemma 1.** [22] *The transformed dynamics (6) has the following properties: 1) The inertia matrix of the transformed dynamics is symmetric and positive definite:  $M_z = M_z^T$ ; 2) The matrix  $(\dot{M}_z - 2C_z)$  is skew-symmetric and fulfills the condition:  $\mathbf{p}^T (\dot{M}_z - 2C_z) \mathbf{p} = 0, \forall \mathbf{p} \in \mathbb{R}^m$ .*

### B. Impedance Control with Prescribed Performance

To integrate impedance control with prescribed performance, we propose a novel impedance model, given by:

$$\begin{aligned} \mathbf{F}_{ez} &= \mathbf{M}_z \ddot{\mathbf{z}} + (\mathbf{D}_d + \mathbf{C}_z) \dot{\mathbf{z}} \\ &\quad + (\mathbf{D}_d \boldsymbol{\lambda}_z + \mathbf{C}_z \boldsymbol{\lambda}_z - \mathbf{M}_z \boldsymbol{\lambda}_z \boldsymbol{\lambda}_z + \mathbf{K}_d) \mathbf{z} \end{aligned} \quad (7)$$

where  $\boldsymbol{\lambda}_z \in \mathbb{R}^{m \times m}$  is a diagonal and positive definite matrix.  $\mathbf{K}_d \in \mathbb{R}^{m \times m}$  and  $\mathbf{D}_d \in \mathbb{R}^{m \times m}$  are constant stiffness and damping. The impedance model (7) aims to achieve two objectives: 1) ensure ultimate boundedness at the position level, thereby preserving position constraints (3); and 2) enable the input command  $\mathbf{F}_z$  to operate without requiring human-robot interaction force sensing. Thus, the command  $\mathbf{F}_z$  is obtained by substituting (7) into (6), as given by:

$$\begin{aligned} \mathbf{F}_z &= -\mathbf{D}_d \boldsymbol{\sigma}_z - (-\mathbf{M}_z \boldsymbol{\lambda}_z \boldsymbol{\lambda}_z + \mathbf{C}_z \boldsymbol{\lambda}_z + \mathbf{K}_d) \mathbf{z} \\ &\quad - \mathbf{F}_\omega + \mathbf{g}_z \end{aligned} \quad (8)$$

where  $\boldsymbol{\sigma}_z = \dot{\mathbf{z}} + \boldsymbol{\lambda}_z \mathbf{z}$  is the sliding manifold.

**Remark 1.** *Traditional impedance models ensure passivity between the velocity error and the interaction force [32], which is insufficient to guarantee ultimate boundedness at the position level. This limitation hinders the integration of conventional impedance control with prescribed performance for enforcing position constraints (3). In contrast, the model (7) is specifically designed to maintain passivity between the position error and the interaction force, thereby enabling the preservation of the position constraints (3). Notably, when  $\boldsymbol{\lambda}_z = 0$ , our model reduces to the classical impedance formulation, highlighting that (7) is a generalized extension.*

**Theorem 1.** *The closed-loop system, governed by (6)-(8), exhibits passivity in the dynamics between the input  $\mathbf{F}_{ez}$  and the output  $\boldsymbol{\sigma}_z$  while preserving the constraints (3), given that*

$$\|\mathbf{F}_{ext}\| < F_m, \lambda_{\min}(\mathbf{D}_d - \mathbf{M}_z \boldsymbol{\lambda}_z) > 0 \quad (9)$$

where  $F_m$  is a positive constant.

*Proof.* A Lyapunov candidate is defined:

$$V_c = \frac{1}{2} \boldsymbol{\sigma}_z^T \mathbf{M}_z \boldsymbol{\sigma}_z + \frac{1}{2} \mathbf{z}^T \mathbf{K}_d \mathbf{z} \quad (10)$$

Its derivative is expressed by:

$$\begin{aligned} \dot{V}_c &= \boldsymbol{\sigma}_z^T (\mathbf{M}_z \ddot{\mathbf{z}} + \mathbf{M}_z \boldsymbol{\lambda}_z \dot{\mathbf{z}}) + \frac{1}{2} \boldsymbol{\sigma}_z^T \dot{\mathbf{M}}_z \boldsymbol{\sigma}_z + \mathbf{z}^T \mathbf{K}_d \dot{\mathbf{z}} \\ &= \boldsymbol{\sigma}_z^T (\mathbf{F}_{ez} - \mathbf{D}_d \boldsymbol{\sigma}_z - \mathbf{C}_z \boldsymbol{\sigma}_z - \mathbf{K}_d \mathbf{z} + \mathbf{M}_z \boldsymbol{\lambda}_z \boldsymbol{\sigma}_z) \\ &\quad + \frac{1}{2} \boldsymbol{\sigma}_z^T \dot{\mathbf{M}}_z \boldsymbol{\sigma}_z + \mathbf{z}^T \mathbf{K}_d \dot{\mathbf{z}} \\ &= \boldsymbol{\sigma}_z^T \mathbf{F}_{ez} - \boldsymbol{\sigma}_z^T (\mathbf{D}_d - \mathbf{M}_z \boldsymbol{\lambda}_z) \boldsymbol{\sigma}_z - \mathbf{z}^T \boldsymbol{\lambda}_z \mathbf{K}_d \mathbf{z} \\ &= -W + \boldsymbol{\sigma}_z^T \mathbf{F}_{ez} \end{aligned} \quad (11)$$

where  $W = \boldsymbol{\sigma}_z^T (\mathbf{D}_d - \mathbf{M}_z \boldsymbol{\lambda}_z) \boldsymbol{\sigma}_z + \mathbf{z}^T \boldsymbol{\lambda}_z \mathbf{K}_d \mathbf{z}$ .

Thus, the passivity of the system is ensured by integrating over the time interval  $[0, t]$  as follows:

$$\int_0^t \boldsymbol{\sigma}_z^T \mathbf{F}_{ez} d\zeta = \int_0^t W d\zeta + V_c(t) - V_c(0) \quad (12)$$

Furthermore, given the relationship  $\|\mathbf{F}_{ez}\| = \|\boldsymbol{\Psi}^T \mathbf{F}_{ext}\| \leq \|\boldsymbol{\Psi}\| \|\mathbf{F}_{ext}\| \leq F_m \|\boldsymbol{\Psi}\|$ , we have:

$$\begin{aligned} \dot{V}_c &\leq \|\mathbf{F}_{ez}\| \|\boldsymbol{\sigma}_z\| - \lambda_{\min}(\mathbf{D}_d - \mathbf{M}_z \boldsymbol{\lambda}_z) \|\boldsymbol{\sigma}_z\|^2 \\ &\quad - \mathbf{z}^T \boldsymbol{\lambda}_z \mathbf{K}_d \mathbf{z} \\ &\leq F_m \|\boldsymbol{\Psi}\| \|\boldsymbol{\sigma}_z\| - \lambda_{\min}(\mathbf{D}_d - \mathbf{M}_z \boldsymbol{\lambda}_z) \|\boldsymbol{\sigma}_z\|^2 \\ &\leq -\|\boldsymbol{\sigma}_z\| (\lambda_{\min}(\mathbf{D}_d - \mathbf{M}_z \boldsymbol{\lambda}_z) \|\boldsymbol{\sigma}_z\| - F_m \|\boldsymbol{\Psi}\|) \end{aligned} \quad (13)$$

Hence,  $\|\boldsymbol{\sigma}_z\|$  is ultimately uniformly bounded by:

$$\|\boldsymbol{\sigma}_z\| \leq \frac{\|\boldsymbol{\Psi}\|}{\lambda_{\min}(\mathbf{D}_d - \mathbf{M}_z \boldsymbol{\lambda}_z)} F_m \quad (14)$$

Defining another Lyapunov candidate  $V_z = \frac{1}{2} \mathbf{z}^T \mathbf{z}$ , yielding its derivative:

$$\begin{aligned} \dot{V}_z &= \mathbf{z}^T \dot{\mathbf{z}} = \mathbf{z}^T (\boldsymbol{\sigma}_z - \boldsymbol{\lambda}_z \mathbf{z}) \\ &\leq -\lambda_{\min}(\boldsymbol{\lambda}_z) \|\mathbf{z}\|^2 + \|\mathbf{z}\| \|\boldsymbol{\sigma}_z\| \end{aligned} \quad (15)$$

$\|\mathbf{z}\|$  is ultimately uniformly bounded by:

$$\|\mathbf{z}\| \leq \frac{\|\boldsymbol{\Psi}\|}{\lambda_{\min}(\boldsymbol{\lambda}_z) \lambda_{\min}(\mathbf{D}_d - \mathbf{M}_z \boldsymbol{\lambda}_z)} F_m \quad (16)$$

The system is globally bounded, and the position constraint (3) is preserved within the defined range.

This completes the proof.  $\square$

## IV. ADAPTIVE VARIABLE IMPEDANCE CONTROL WITH FLEXIBLE PRESCRIBED PERFORMANCE

This paper proposes a variable impedance controller with flexible prescribed performance to balance tracking accuracy and system compliance in the human-robot interaction.

### A. Joint Strength Index

This section aims to define the JSI to represent human motor capabilities. The objective utilizes sEMG to calculate joint torques  $\tau_{hi}$  through a musculoskeletal model that incorporates an elastic tendon in series with the muscle fibers to determine the muscle-tendon force  $F_i^{mt}$  (shown in Fig. 1), given by:

$$F_i^{mt} = (F_{CE,i} + F_{PE,i}) \cos \phi_i \quad (17)$$

where  $\phi_i$  denotes the pennation angle between the orientation of the muscle fiber and tendon.  $F_{PE,i}$  represents the passive elastic element, typically modeled as a nonlinear spring. While  $F_{CE,i}$  denotes the active force generated by the CE and is associated with muscle activation, as expressed as:

$$F_{CE,i} = F_{o,i}^m f_a(\bar{l}_{i,a}^m) f(\bar{v}_i) \alpha_i(t) \quad (18)$$

$$F_{PE,i} = F_{o,i}^m f_p(\bar{l}_{i,a}^m) \quad (19)$$

where  $F_{o,i}^m$  is the maximum isometric force.  $f_a(\bar{l}_{i,a}^m)$  represents the active force-length relationship as a function of the normalized muscle fiber length,  $\bar{l}_{i,a}^m$ . This normalized length,  $\bar{l}_{i,a}^m$ , is obtained by scaling the muscle fiber length  $l_i^m$  relative to muscle activation and the optimal muscle fiber length  $l_{o,i}^m$ .  $f(\bar{v}_i)$  represents the force-velocity relationship between the muscle fiber length  $l_i^m$  and the normalized contraction velocity  $\bar{v}_i$ .  $\bar{l}_{i,a}^m$  denotes the ratio of muscle-fiber length to the optimal

muscle-fiber length.  $\alpha_i(t)$  is the muscle activation with respect to the pre-processed sEMG signal [33], given by:

$$\alpha_i(t) = \frac{e^{A I_{EMG,i}(t)} - 1}{e^A - 1} \quad (20)$$

where non-linear shape factor  $A$  has the range of highly nonlinearity (-3) to linearity (0.01).

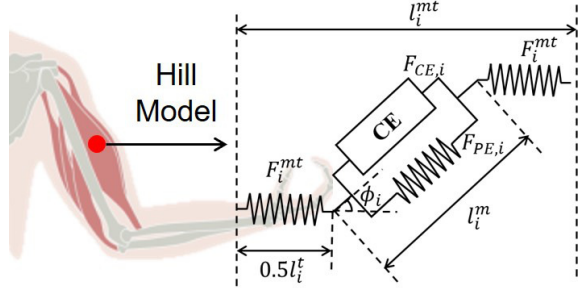


Fig. 1. A musculoskeletal model with Hill-type muscle.

Thus, the torque  $\tau_{hi}$  generated by each muscle can be determined using  $F_i^{mt}$  and the moment arm  $r_i$  for the joint angle, and the torque at a single joint can be determined by :

$$\tau_{hi} = \sum_i F_i^{mt} r_i, \varphi_i = \frac{1}{1 + \exp(-\beta_i(\tau_{hi} - \tau_{mi}))} \quad (21)$$

where  $\tau_{mi}$  is the median value of the torque.  $\beta_i$  is a positive constants.  $0 < \varphi_i < 1$  represents the JSI, quantifying the degree of active torque exerted by the user.

## B. Controller Adaption

1) *Flexible Prescribed Performance*: The prescribed performance focuses on regulating the positional constraint range, taking human participation into account, as detailed below:

$$\rho_{i\infty} = \delta_{i0} + (\delta_{i1} - \delta_{i0})\varphi_i \quad (22)$$

where  $\delta_{i0}$  and  $\delta_{i1}$  are the minimum and maximum values of the constraint range, respectively.

This flexible prescribed performance reflects that as the degree of active human participation increases, the system's reliance on human behavior gradually strengthens, leading to an expansion of the constraint range. This allows for greater freedom to accommodate the needs of active human motion. Conversely, when the level of active human participation is low, the system needs to provide more guidance and support, resulting in a reduction of the constraint range to ensure the motion accuracy and safety.

2) *Impedance Adaption*: The stiffness and damping adaption are designed to establish human-dominant and robot-dominant modes while ensuring smooth transitions between them, given by

$$\begin{cases} \mathbf{K} = \mathbf{K}_a + \mathbf{K}_d \\ \dot{\mathbf{K}}_a = (\mathbf{I} - \Phi)\varsigma_K \sigma_z z^T - \Phi \mathbf{v}_K \mathbf{K}_a \end{cases} \quad (23)$$

$$\begin{cases} \mathbf{D} = \mathbf{D}_a + \mathbf{D}_d \\ \dot{\mathbf{D}}_a = (\mathbf{I} - \Phi)\varsigma_D \sigma_z \dot{z}^T - \Phi \mathbf{v}_D \mathbf{D}_a \end{cases} \quad (24)$$

where  $\Phi = \text{diag}\{\varphi_1, \dots, \varphi_m\} \in \mathbb{R}^{m \times m}$ .  $\varsigma_K \in \mathbb{R}^{m \times m}$ ,  $\mathbf{v}_K \in \mathbb{R}^{m \times m}$ ,  $\varsigma_D \in \mathbb{R}^{m \times m}$ ,  $\mathbf{v}_D \in \mathbb{R}^{m \times m}$  are definite

constant matrices.  $\mathbf{K}_a \in \mathbb{R}^{m \times m}$  and  $\mathbf{D}_a \in \mathbb{R}^{m \times m}$  are time-varying terms of the stiffness and damping.  $\mathbf{K}_a(0) = \mathbf{K}_{a0}$  and  $\mathbf{D}_a(0) = \mathbf{D}_{a0}$  are positive definite matrices.  $\mathbf{K}_d \in \mathbb{R}^{m \times m}$  and  $\mathbf{D}_d \in \mathbb{R}^{m \times m}$  are positive definite constant matrices.

The analysis of the adaptation of stiffness and damping is provided below:

- $\sigma_z z^T$  and  $\sigma_z \dot{z}^T$  are positive gain terms in  $\mathbf{K}_a$  and  $\mathbf{D}_a$ , when the converging rate  $z^T \dot{z} > -z^T \lambda_z z$  and  $\dot{z}^T \lambda_z z > -\dot{z}^T \dot{z}$ . Meanwhile,  $-\mathbf{v}_K \mathbf{K}_a$  and  $-\mathbf{v}_D \mathbf{D}_a$  serve as decay terms that prevent  $\mathbf{K}_a$  and  $\mathbf{D}_a$  from growing unbounded.
- $\Phi$  acts as an indicator of human joint strength, primarily building the human-dominated and robot-dominated modes, and enabling smooth transitions between them.

**Remark 2.**  $\Phi$  is crucial for building the human-dominated and robot-dominated modes. When  $\Phi$  approaches  $\mathbf{0}$ ,  $\dot{\mathbf{K}}_a$  and  $\dot{\mathbf{D}}_a$  are predominantly influenced by the positive gain terms, specifically  $\varsigma_K \sigma_z z^T$  and  $\varsigma_D \sigma_z \dot{z}^T$ , resulting in an increase in  $\mathbf{K}$  and  $\mathbf{D}$ . This increase enhances the system's ability to track the desired trajectory, representing the robot-dominant mode. Conversely, as  $\Phi$  approaches  $\mathbf{I}$ , the decay terms, specifically  $-\mathbf{v}_K \mathbf{K}_a$  and  $-\mathbf{v}_D \mathbf{D}_a$ , become the dominant factors in  $\dot{\mathbf{K}}_a$  and  $\dot{\mathbf{D}}_a$ , leading to a decrease in  $\mathbf{K}$  and  $\mathbf{D}$ , which corresponds to the human-dominant mode. Furthermore, as  $\Phi$  is a continuous function, the system ensures smooth and seamless transitions between human-dominant and robot-dominant modes to ensure the stability of human-robot interaction.

**Lemma 2.** If  $[z^T, \dot{z}^T]^T$  is ultimately uniformly bounded,  $\mathbf{K}_a$  and  $\mathbf{D}_a$  are positive definite, with  $\|\mathbf{K}_a\|$  and  $\|\mathbf{D}_a\|$  bounded by specified limits, given by

$$\lambda_{KD} = \frac{\|\Lambda\|}{\min(\lambda_{\min}(\Phi \mathbf{v}_K), \lambda_{\min}(\Phi \mathbf{v}_D))} \quad (25)$$

where  $\Lambda = [ \|(\mathbf{I} - \Phi)\varsigma_K\| \|\sigma_z z^T\|, \|(\mathbf{I} - \Phi)\varsigma_D\| \|\sigma_z \dot{z}^T\| ]^T$ .

*Proof.* Let  $V_K$  be a Lyapunov candidate defined as  $V_K = \frac{1}{2} \|\mathbf{K}_a\|_F^2 + \frac{1}{2} \|\mathbf{D}_a\|_F^2$ , yielding its derivative as follows:

$$\begin{aligned} \dot{V}_K &= \text{tr}(\mathbf{K}_a^T \dot{\mathbf{K}}_a) + \text{tr}(\mathbf{D}_a^T \dot{\mathbf{D}}_a) \\ &= \text{tr}(\mathbf{K}_a^T (\mathbf{I} - \Phi)\varsigma_K \sigma_z z^T) - \text{tr}(\mathbf{K}_a^T \Phi \mathbf{v}_K \mathbf{K}_a) \\ &\quad + \text{tr}(\mathbf{D}_a^T (\mathbf{I} - \Phi)\varsigma_D \sigma_z \dot{z}^T) - \text{tr}(\mathbf{D}_a^T \Phi \mathbf{v}_D \mathbf{D}_a) \\ &\leq \|(\mathbf{I} - \Phi)\varsigma_K\| \|\sigma_z z^T\| \|\mathbf{K}_a\| - \lambda_{\min}(\Phi \mathbf{v}_K) \|\mathbf{K}_a\|^2 \\ &\quad + \|(\mathbf{I} - \Phi)\varsigma_D\| \|\sigma_z \dot{z}^T\| \|\mathbf{D}_a\| - \lambda_{\min}(\Phi \mathbf{v}_D) \|\mathbf{D}_a\|^2 \\ &= \Lambda^T \Theta - \Theta^T \begin{bmatrix} \lambda_{\min}(\Phi \mathbf{v}_K) & 0 \\ 0 & \lambda_{\min}(\Phi \mathbf{v}_D) \end{bmatrix} \Theta \\ &\leq \|\Lambda\| \|\Theta\| - \min(\lambda_{\min}(\Phi \mathbf{v}_K), \lambda_{\min}(\Phi \mathbf{v}_D)) \|\Theta\|^2 \end{aligned} \quad (26)$$

where  $\Theta = [ \|\mathbf{K}_a\|, \|\mathbf{D}_a\| ]^T$ . If  $[z^T, \dot{z}^T]^T$  is ultimately uniformly bounded,  $\|\Lambda\|$  and  $\|\sigma_z\|$  are bounded, indicating that  $\|\mathbf{K}_a\|$  and  $\|\mathbf{D}_a\|$  are bounded by  $\lambda_{KD}$ .

Given that  $\mathbf{K}_a(0)$  and  $\mathbf{D}_a(0)$  are positive definite, when  $\|\mathbf{K}_a\|$  or  $\|\mathbf{D}_a\|$  decreases, making  $\|\mathbf{K}_a\|$  or  $\|\mathbf{D}_a\|$  less than  $\lambda_{KD}$ , this results in  $\dot{V}_K > 0$ , thereby causing  $\|\mathbf{K}_a\|$  or  $\|\mathbf{D}_a\|$  to increase. This response effectively prevents  $\mathbf{K}_a$  and  $\mathbf{D}_a$  from decreasing to become negative definite.

This completes the proof.  $\square$

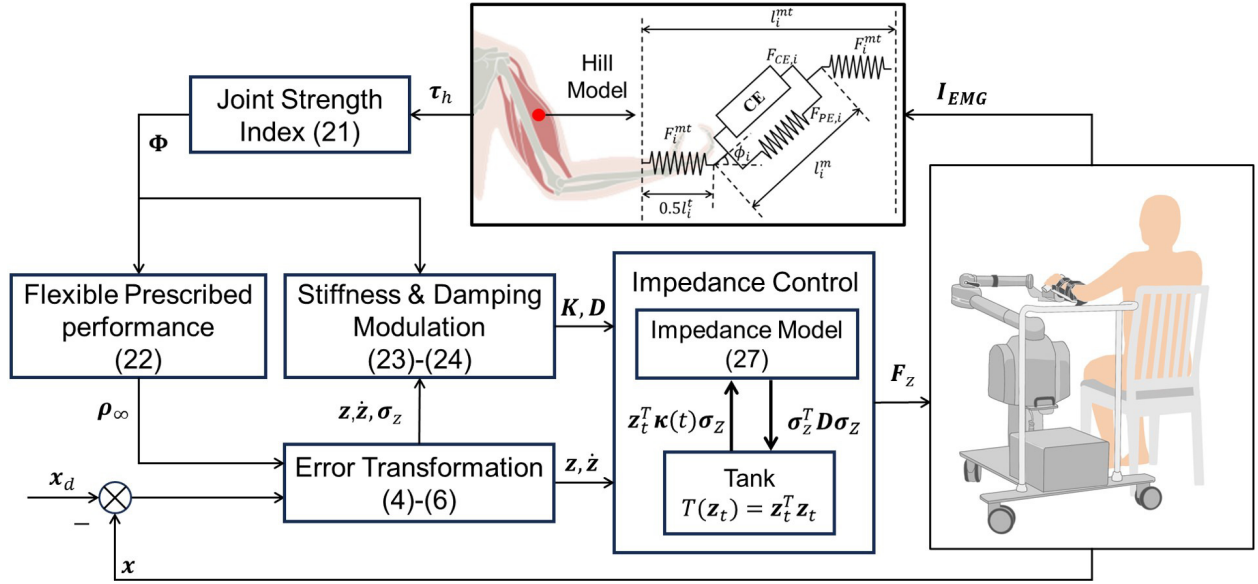


Fig. 2. Control system diagram.

### C. Tank-based Stability Guarantee

Variable stiffness signifies a departure from system passivity, as the variations in stiffness introduces additional energy into the system. A solution is to create an energy tank that retrieves the energy dissipated from  $\dot{z}^T D_d \dot{z}$  [32]. The energy stored in the tank, represented by  $T(z_t) = \frac{1}{2} z_t^T z_t$  with an internal state vector  $z_t \in \mathbb{R}^m$ . The energy exchange between the tank and the new impedance model is governed by:

$$F_{ez} = M_z \ddot{z} + (D + C_z) \dot{z} \quad (27)$$

$$+ (D \lambda_z + C_z \lambda_z - M_z \lambda_z \lambda_z + K_d) z - \kappa(t) z_t \quad (28)$$

$$\dot{z}_t = z_t^{-T} \sigma_z^T \Gamma D \sigma_z - \kappa(t) \sigma_z$$

where  $\Gamma$  governs the charging rate of the tank.  $z_t^{-T}$  denotes the transpose of the pseudo-inverse of  $z_t$ .  $\kappa(t)$  represents the variable stiffness coefficient that regulates the energy exchange between the impedance model and the tank, expressed as:

$$\kappa(t) = \begin{cases} \mathbf{0}, & T(z_t) < \bar{T} \\ -K_a z z_t^{-1}, & \text{otherwise} \end{cases} \quad (29)$$

When the energy level within the tank is insufficient, the impedance model transitions from variable stiffness to fixed stiffness. This prevents further energy injection into the system, thereby avoiding the singularity described in (28).

**Theorem 2.** *The closed-loop system with variable impedance described by (6)-(8) exhibits the passivity of the dynamics between the input torque  $F_{ez}$  and the output  $\sigma_z$ , and preserves the position constraints (3) given that*

$$\lambda_{\min}((I - \Gamma) D - M_z \lambda_z) > 0 \quad (30)$$

*Proof.* A new Lyapunov candidate is defined, given by  $V_c^t = V_c + T(z_t)$ . Its derivative can be expressed as:

$$\begin{aligned} \dot{V}_c^t &= \sigma_z^T (M_z \ddot{z} + M_z \lambda_z \dot{z}) + \frac{1}{2} \sigma_z^T \dot{M}_z \sigma_z \quad (31) \\ &+ z^T K_d \dot{z} + z_t^T \dot{z}_t \\ &= \sigma_z^T F_{ez} - \sigma_z^T (D - M_z \lambda_z) \sigma_z - z^T \lambda_z K_d z \\ &+ \sigma_z^T \kappa(t) z_t + \sigma_z^T \Gamma D \sigma_z - z_t^T \kappa(t) \sigma_z \\ &= \sigma_z^T F_{ez} - \sigma_z^T ((I - \Gamma) D - M_z \lambda_z) \sigma_z - z^T \lambda_z K_d z \\ &= -W^t + \sigma_z^T F_{ez} \end{aligned}$$

where  $W^t = \sigma_z^T ((I - \Gamma) D - M_z \lambda_z) \sigma_z + z^T \lambda_z K_d z$ . The passivity of the system with variable impedance is ensured.

By using the similar techniques in Proof of Theorem 1,  $\|\sigma_z\|$  and  $\|z\|$  are ultimately uniformly bounded by:

$$\|\sigma_z\| \leq \frac{\|\Psi\|}{\lambda_{\min}((I - \Gamma) D - M_z \lambda_z)} F_m \quad (32)$$

$$\|z\| \leq \frac{\|\Psi\|}{\lambda_{\min}(\lambda_z) \lambda_{\min}((I - \Gamma) D - M_z \lambda_z)} F_m \quad (33)$$

This completes the proof.  $\square$

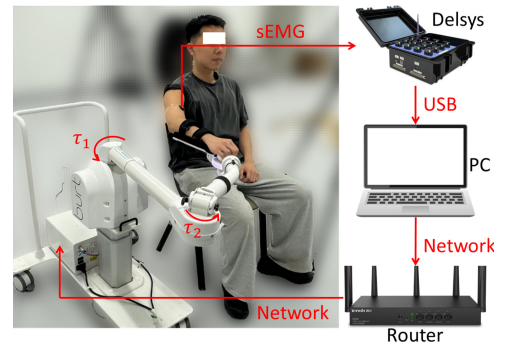


Fig. 3. Upper limb rehabilitation robot.

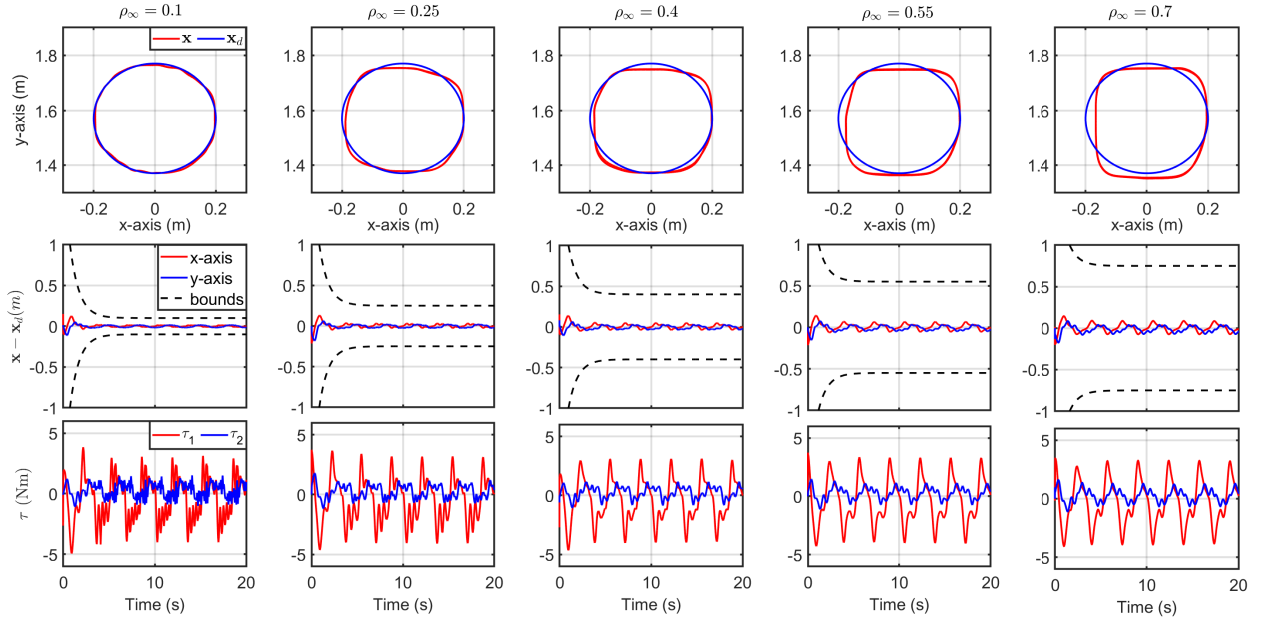


Fig. 4. System performance with fixed stiffness and damping under varying  $\rho_\infty$ : The first row displays the tracking performance under various  $\rho_\infty$ . The second row illustrates the tracking error with position constraints. The third row presents the corresponding control signal.

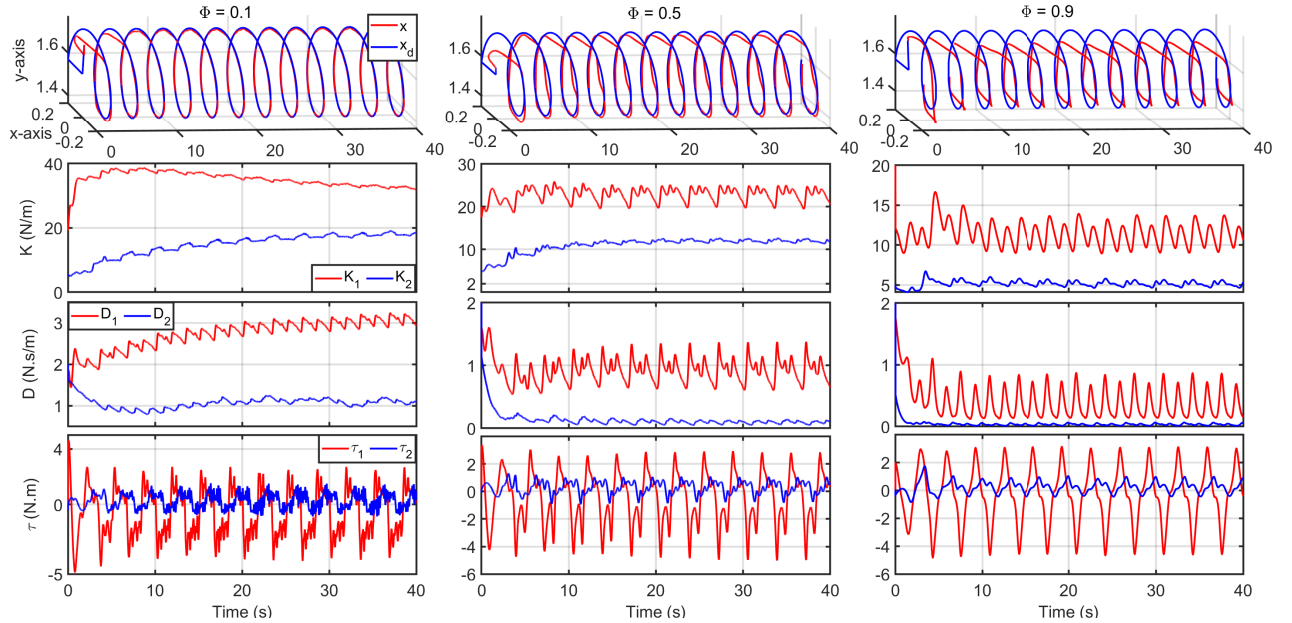


Fig. 5. System performance with adaptive stiffness and damping under varying  $\Phi$ . The first row represents the tracking performance, the second row shows the stiffness variations, the third row illustrates the damping adjustments, and the fourth row depicts the control inputs.

## V. EXPERIMENTAL STUDIES

### A. Experimental Setup

This method has been implemented on a 3-DOF upper-limb cable-driven rehabilitation robot named Burt, developed by ESTUN Medical Robot Technology Co., Ltd., as shown in Fig. 3. The human-robot interaction occurs at the end-effector, without force sensing. In the experiments, we primarily focus on the two DOF near the end-effector to evaluate the system's performance. The robot allows direct control via a network interface for adjusting joint torques, operating at a sampling

interval of 0.002 seconds.

A healthy participant (age: 24, sex: male, height: 185 cm, weight: 83 kg) took part in the experiments. The ethics approval for experiments with healthy subjects was granted by the Engineering and Physical Sciences Faculty Research Ethics Committee of the University of Leeds (LTELEC-001). This paper focuses on sEMG measurements at the elbow joint, collecting two-channel signals from the biceps and triceps brachii using Delsys Trigno<sup>TM</sup> system, with a sampling frequency of 2148 Hz. The raw sEMG signals are first filtered with a second-order Butterworth band-pass filter, set between 25 Hz

and 450 Hz, to remove noise and artifacts. Next, a fourth-order Butterworth low-pass filter with a corner frequency of 4 Hz is applied to clarify the relationship between the sEMG signals and muscle force. Finally, the filtered signals are normalized by dividing by the peak value of the isometric maximum voluntary contraction (IMVC). Using the musculoskeletal model from Section IV.A, optimized with the technique in [34], the elbow joint torque  $\tau_h$  is calculated and transmitted to the robot control board over a network interface at 1058 Hz.

## B. Experimental Results

1) *Fixed Assistance Scenario*: The objective is to establish a passive rehabilitation scenario for the patient, utilizing the approach described in Section III. In this scenario, the volunteer simulates the patient's muscle weakness, allowing the robot to guide the movement of the arms. Five Experimental trials were conducted with prescribed performance parameter  $\rho_{0i} = 2$  and  $k_i = 1$  along with various  $\rho_\infty = \{0.1, 0.25, 0.4, 0.55, 0.7\}$ . The fixed stiffness and damping parameters are set to  $\mathbf{K}_d = \text{diag}\{35, 10\} (N \cdot m)$  and  $\mathbf{D}_d = \text{diag}\{0.5, 0.5\} (N \cdot s/m)$ . The experimental results are shown in Fig. 4 to demonstrate system performance.

When  $\rho_\infty = 0.1$ , the system demonstrates relatively high tracking precision. The control signal exhibits significant chattering, indicating increased sensitivity to error signals. In contrast, when  $\rho_\infty = 0.25$  and  $\rho_\infty = 0.4$ , the tracking performance declines significantly, and the intensity of the control signal's chattering also decreases noticeably. Furthermore, at  $\rho_\infty = 0.55$  and  $\rho_\infty = 0.7$ , tracking performance further deteriorates, yet the intensity of the control vibrations shows no significant change compared to the previous cases. This indicates that a smaller  $\rho_\infty$  leads to stronger vibrations in the control signal, resulting in higher tracking accuracy. However, a small  $\rho_\infty$  enhances the system's tracking accuracy but reduces compliance, causing the algorithm to prioritize position control over responding to external forces.

2) *Assist-As-Needed Scenario*: The goal of this section is to create an assist-as-needed scenario using the techniques from Section IV. This experiment is divided into two phases: 1) We manually set the value of JSI to validate the design of  $\hat{\mathbf{K}}_a$  and  $\hat{\mathbf{D}}_a$ . 2) Through real-time computation of the JSI, we assess the AAN strategy's ability to balance compliance and motion precision in the human-robot interaction. The experimental parameters are set as follows:  $\varsigma_K = \text{diag}\{400, 500\}$ ,  $\mathbf{v}_K = \text{diag}\{0.5, 0.1\}$ ,  $\varsigma_D = \text{diag}\{15, 5\}$ , and  $\mathbf{v}_D = \text{diag}\{0.8, 2\}$ .

In the first phase, we manually selected  $\Phi = \{0.1, 0.5, 0.9\}$ , corresponding to low, moderate, and high levels of human involvement. The experimental results are shown in Fig. 5. It can be observed that under a fixed  $\Phi$ , the stiffness and damping adaptively adjust and stabilize, with their values remaining greater than zero, confirming the validity of Lemma 2. Also, as  $\Phi$  increases, the system's stiffness and damping significantly decrease, leading to a decline in tracking performance and a noticeable reduction in the vibration intensity of the control inputs. This indicates that high human involvement enhances the system's compliance, which reduces tracking precision but enables the system to respond to external forces, representing

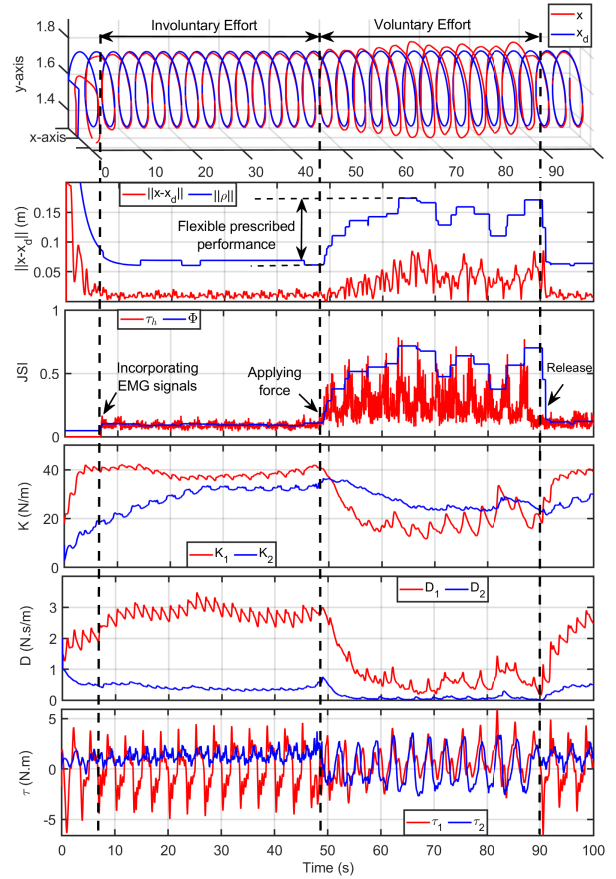


Fig. 6. Time evolution of human-robot interaction. The process consists of three phases: 1) The human remains involuntary (6-48 seconds); 2) The human actively applies force to guide the robot along its trajectory (48-90 seconds); 3) The human muscles relax, returning to an involuntary state. (90-100 seconds).

a human-dominated mode. In contrast, low human involvement increases the system's stiffness, enabling high-precision motion, but the system becomes unable to respond to external forces, typically representing a robot-dominated mode. Furthermore, moderate human involvement strikes a balance between high and low involvement, maintaining compliance while ensuring a certain level of movement precision. Thus, when the human involvement can be adjusted in real-time based on  $\Phi$ , the approach may effectively balance tracking accuracy and system compliance.

In the second phase, the process involves the successive transformation of human voluntary actions: from involuntary effort to voluntary effort, and then back to involuntary effort. Once the system begins operation, the human stays passive, with the robot driving the movement for totally 48 seconds. Immediately following, the human actively applies force, attempting to guide the robot's end effector along the original trajectory for another 42 seconds. Finally, the human muscles relax and return to a passive state. The experimental results are shown in Fig. 6. After integrating sEMG signals (6-48 seconds), the human remains involuntary, resulting in low-level human involvement, as reflected by JSI-related metrics. Adaptive adjustments in  $\mathbf{K}$  and  $\mathbf{D}$  lead to increased stiffness, ensuring high tracking accuracy while maintaining a narrower

prescribed performance range (see  $\|\mathbf{x} - \mathbf{x}_d\|$  and  $\|\rho\|$ ). The pronounced chattering in the control input indicates that the system is primarily focused on precise trajectory tracking. This is typically a robot-dominated mode. In the subsequent voluntary effort phase (48-90 seconds), the human applies force to guide the robot along the original trajectory. This leads to a significant increase in  $\Phi$ , which consequently reduces  $\mathbf{K}$  and  $\mathbf{D}$ . This adjustment makes the system more responsive to external force. However, humans often struggle to guide robots precisely along the original path, causing  $\|\mathbf{x} - \mathbf{x}_d\|$  to increase significantly, and the prescribed performance range  $\|\rho\|$  expands, allowing for greater freedom in human movement. This indicates that the system prioritizes human dominance according to  $\Phi$ . Finally, when the human ceases exerting muscle force (90-100 seconds), the system transitions back to precise trajectory tracking. Note that the stiffness and damping in this experiment are relatively small, mainly due to the following reasons: 1)  $e_x$  is nonlinearly transformed into  $z$ , implying that  $\mathbf{K}$  and  $\mathbf{D}$  represent the equivalent stiffness and damping rather than the physical stiffness and damping. 2) The cable-driven rehabilitation robot, compared to industrial robots, prioritizes compliance in human-robot interaction.

This dynamic process demonstrates an effective balance between compliance and tracking accuracy by adapting to the varying strength of human joints. This effectively enhances the overall performance of human-robot interactions, improving rehabilitation outcomes and enabling more personalized, adaptive training. However, the current validation is limited to healthy individuals. We recognize that significant physiological and neuromuscular differences exist between healthy subjects and rehabilitation patients. Key limitations include: 1) The method assumes that subjects have at least some residual muscle activity for force estimation and control adaptation; 2) The musculoskeletal model is based on standard joint dynamics and may not accurately reflect severe pathological conditions such as contractures, hypertonia, or joint deformities; 3) Patients with unpredictable neuromuscular responses (e.g., spasms) may not be accurately represented by the current musculoskeletal model; 4) Although the control approach offers a sound theoretical basis, further integration with patient-specific clinical data is necessary to enable precise individualization and improve clinical applicability.

## VI. CONCLUSION

This paper presents an sEMG-driven musculoskeletal model-based adaptive variable impedance control with flexible prescribed performance for rehabilitation robots. First, we introduce a novel impedance model that integrates prescribed performance and impedance control techniques. Furthermore, by real-time measurement of human involvement using an sEMG-driven musculoskeletal model, this approach constructs a flexible prescribed performance function and adaptive stiffness-damping. A series of experiments were conducted on an upper limb rehabilitation robot, and the results showed that the method seamlessly transitions between human-dominated and robot-dominated modes, effectively balancing the system's tracking accuracy and compliance. Future efforts will aim to

extend the applicability of the proposed method to rehabilitation patients exhibiting a range of neuromuscular impairments. This includes addressing reduced muscle activity, abnormal joint conditions, and variable motor responses. A critical next step will involve incorporating patient-specific clinical data to improve personalization and clinical utility.

## REFERENCES

- [1] P. Langhorne, J. Bernhardt, and G. Kwakkel, "Stroke rehabilitation," *The Lancet*, vol. 377, no. 9778, pp. 1693–1702, 2011.
- [2] C. M. Stinear, C. E. Lang, S. Zeiler, and W. D. Byblow, "Advances and challenges in stroke rehabilitation," *The Lancet Neurology*, vol. 19, no. 4, pp. 348–360, 2020.
- [3] M. Costandi, "Rehabilitation: Machine recovery," *Nature*, vol. 510, no. 7506, pp. S8–S9, 2014.
- [4] Y. Cao and J. Huang, "Neural-network-based nonlinear model predictive tracking control of a pneumatic muscle actuator-driven exoskeleton," *IEEE-CAA J. Automatica Sin.*, vol. 7, no. 6, pp. 1478–1488, Nov. 2020.
- [5] A. D. Banyai and C. Briřan, "Robotics in physical rehabilitation: Systematic review," *Healthcare*, vol. 12, no. 17, 2024.
- [6] B. Brahmi *et al.*, "Novel adaptive impedance control for exoskeleton robot for rehabilitation using a nonlinear time-delay disturbance observer," *ISA Trans.*, vol. 108, pp. 381–392, 2021.
- [7] S. Hussain, S. Q. Xie, and P. K. Jamwal, "Adaptive impedance control of a robotic orthosis for gait rehabilitation," *IEEE Trans. Cybern.*, vol. 43, no. 3, pp. 1025–1034, Jun. 2013.
- [8] P. K. Jamwal *et al.*, "Impedance control of an intrinsically compliant parallel ankle rehabilitation robot," *IEEE Trans. Ind. Electron.*, vol. 63, no. 6, pp. 3638–3647, Jun. 2016.
- [9] H. Ma, Q. Zhou, H. Li, and R. Lu, "Adaptive prescribed performance control of a flexible-joint robotic manipulator with dynamic uncertainties," *IEEE Trans. Cybern.*, vol. 52, no. 12, pp. 12905–12915, Dec. 2022.
- [10] Z. Xu, W. Deng, H. Shen, and J. Yao, "Extended-state-observer-based adaptive prescribed performance control for hydraulic systems with full-state constraints," *IEEE-ASME Trans. Mechatron.*, vol. 27, no. 6, pp. 5615–5625, Dec. 2022.
- [11] Y. Cao *et al.*, "Prescribed performance control of a link-type exoskeleton powered by pneumatic muscles with virtual elasticity," *Nonlinear Dyn.*, vol. 112, pp. 10043–10060, 2024.
- [12] A. Irawan *et al.*, "Interaction motion on pneumatic cylinder using prescribed performance force tracking impedance control," in *2020 8th Int. Conf. Control, Mechatronics Autom. (ICCA)*, pp. 121–126, Moscow, Russia, 2020.
- [13] X. Gu, L. Liu, L. Wang, J. Mao, and Y. Guo, "Predefined-time impedance control of free-flying flexible-joint space robots for force sensor-less target capturing with prescribed performance," *Int. J. Robot Nonlinear Control*, vol. 35, no. 2, pp. 452–478, 2024.
- [14] Q. Meng and Y. Lin, "Adaptive admittance tracking control for interactive robot with prescribed performance," *J. Syst. Eng. Electron.*, vol. 35, no. 2, pp. 444–450, 2024.
- [15] L. L. Cai *et al.*, "Assist-as-needed training paradigms for robotic rehabilitation of spinal cord injuries," in *Proc. 2006 IEEE Int. Conf. Robot. Autom. (ICRA)*, pp. 3504–3511, Orlando, FL, USA, 2006.
- [16] A. U. Pehlivan, D. P. Losey, and M. K. O'Malley, "Minimal assist-as-needed controller for upper limb robotic rehabilitation," *IEEE Trans. Robot.*, vol. 32, no. 1, pp. 113–124, Feb. 2016.
- [17] E. T. Wolbrecht *et al.*, "Optimizing compliant, model-based robotic assistance to promote neurorehabilitation," *IEEE Trans. Neural Syst. Rehabil. Eng.*, vol. 16, no. 3, pp. 286–297, Jun. 2008.
- [18] A. Duschau-Wicke *et al.*, "Path control: A method for patient-cooperative robot-aided gait rehabilitation," *IEEE Trans. Neural Syst. Rehabil. Eng.*, vol. 18, no. 1, pp. 38–48, Feb. 2010.
- [19] P. Agarwal and A. D. Deshpande, "Subject-specific assist-as-needed controllers for a hand exoskeleton for rehabilitation," *IEEE Robot. Autom. Lett.*, vol. 3, no. 1, pp. 508–515, Jan. 2018.
- [20] H. J. Asl, M. Yamashita, T. Narikiyo, and M. Kawanishi, "Field-based assist-as-needed control schemes for rehabilitation robots," *IEEE-ASME Trans. Mechatron.*, vol. 25, no. 4, pp. 2100–2111, Aug. 2020.
- [21] N. Garcia-Hernandez, C. Munguia-Angeles, and V. Parra-Vega, "Assist-as-needed robotic strategy based on velocity fields for enhancing motor training," *IEEE-ASME Trans. Mechatron., Early Access*, DOI 10.1109/TMECH.2024.3445314, 2024.

- [22] Y. Cao, X. Chen, M. Zhang, and J. Huang, "Adaptive position constrained assist-as-needed control for rehabilitation robots," *IEEE Trans. Ind. Electron.*, vol. 71, no. 4, pp. 4059–4068, Apr. 2024.
- [23] M. Sharifi *et al.*, "Impedance variation and learning strategies in human-robot interaction," *IEEE Trans. Cybern.*, vol. 52, no. 7, pp. 6462–6475, Jul. 2022.
- [24] F. J. Abu-Dakka and M. Saveriano, "Variable impedance control and learning: A review," *Front. Robot. AI*, vol. 7, p. 590681, 2020.
- [25] M. Maaref, A. Rezazadeh, K. Shamaei, R. Ocampo, and T. Mahdi, "A bicycle cranking model for assist-as-needed robotic rehabilitation therapy using learning from demonstration," *IEEE Robot. Autom. Lett.*, vol. 1, no. 2, pp. 653–660, Jul. 2016.
- [26] Z. Jin, A. Liu, W. a. Zhang, and L. Yu, "An optimal variable impedance control with consideration of the stability," *IEEE Robot. Autom. Lett.*, vol. 7, no. 2, pp. 1737–1744, Apr. 2022.
- [27] Y. Zhang, S. Li, K. J. Nolan, and D. Zanutto, "Adaptive assist-as-needed control based on actor-critic reinforcement learning," in *2019 IEEE/RSJ Int. Conf. Intell. Robots Syst. (IROS)*, pp. 4066–4071, Macau, China, 2019.
- [28] Y. Zhang, S. Li, K. J. Nolan, and D. Zanutto, "Reinforcement learning assist-as-needed control for robot assisted gait training," in *2020 8th IEEE RAS/EMBS Int. Conf. Biomed. Robot. Biomechatron. (BioRob)*, pp. 785–790, New York, NY, USA, 2020.
- [29] S. Pareek, H. J. Nisar, and T. Kesavadas, "Ar3n: A reinforcement learning-based assist-as-needed controller for robotic rehabilitation," *IEEE Robot. Autom. Mag.*, vol. 31, no. 3, pp. 74–82, Sept. 2024.
- [30] J. Yang, T. Sun, L. Cheng, and Z.-G. Hou, "Spatial repetitive impedance learning control for robot-assisted rehabilitation," *IEEE-ASME Trans. Mechatron.*, vol. 28, no. 3, pp. 1280–1290, Jun. 2023.
- [31] M. Sharifi, V. Azimi, V. K. Mushahwar, and M. Tavakoli, "Impedance learning-based adaptive control for human-robot interaction," *IEEE Trans. Control Syst. Technol.*, vol. 30, no. 4, pp. 1345–1358, Jul. 2022.
- [32] F. Ferraguti, C. Secchi, and C. Fantuzzi, "A tank-based approach to impedance control with variable stiffness," in *2013 IEEE Int. Conf. Robot. Autom.*, pp. 4948–4953, Karlsruhe, Germany, 2013.
- [33] T. S. Buchanan *et al.*, "Neuromusculoskeletal modeling: Estimation of muscle forces and joint moments and movements from measurements of neural command," *J. Appl. Biomech.*, vol. 20, no. 4, pp. 367 – 395, 2004.
- [34] Y. Zhao *et al.*, "An emg-driven musculoskeletal model for estimating continuous wrist motion," *IEEE Trans. Neural Syst. Rehabil. Eng.*, vol. 28, no. 12, pp. 3113–3120, 2020.